The use of random forests to identify brain regions on amyloid and FDG PET associated with MoCA score

Katherine Zukotynski, MD, PhD, McMaster University, Hamilton, ON, Canada
Vincent Gaudet, PhD, University of Waterloo, Waterloo, ON, Canada
Phillip H. Kuo, MD, PhD, University of Arizona, Tucson, AZ, USA
Sabrina Adamo, HBSc, Sunnybrook Research Institute, Toronto, ON, Canada
Maged Goubran, PhD, Sunnybrook Research Institute, Toronto, ON, Canada
Christopher Scott, BScH, Sunnybrook Research Institute, Toronto, ON, Canada
Christian Bocti, MD, Université de Sherbrooke, Sherbrooke, QC, Canada
Michael Borrie, MB ChB, Western University, London, ON, Canada
Howard Chertkow, MD, Jewish General Hospital, Montreal, QC, Canada
Richard Frayne, PhD, University of Calgary, Calgary, AB, Canada
Robin Hsiung, MD, University of British Columbia, Vancouver, BC, Canada
Robert Laforce, Jr., MD, PhD, Université Laval, Québec, QC, Canada
Michael D. Noseworthy, PhD, McMaster University, Hamilton, ON, Canada
Frank S. Prato, PhD, Western University, London, ON, Canada
Demetrios J. Sahlas, MD, McMaster University, Hamilton, ON, Canada
Eric E. Smith, MD, MPH, Hotchkiss Brain Institute, University of Calgary, Calgary, AB, Canada
Vesna Sossi, PhD, University of British Columbia, Vancouver, BC, Canada
Alexander Thiel, MD, Jewish General Hospital, Montreal, QC, Canada
Jean-Paul Soucy, MD, Montreal Neurological Institute, Montreal, QC, Canada
Jean-Claude Tardif, MD, Montreal Heart Institute, Université de Montréal, Montreal, QC, Canada
Sandra E. Black, MD, Department of Medicine (Neurology), Sunnybrook Health Sciences Centre and Sunnybrook Research Institute, University of Toronto, Toronto, ON, Canada

Name and address for correspondence:
Katherine Zukotynski
Address: McMaster University, 1200 Main St. W., Rm. 1P11, Hamilton, ON L8P 3Z5 Canada
Fax: 905-577-1443
Phone: 647-926-0194
Email: katherine.zukotynski@utoronto.ca

Short title: Random forests to explore associations of MoCA score with amyloid and FDG PET

The use of random forests to identify brain regions on amyloid and FDG PET associated with MoCA score

Abstract

Purpose: To evaluate random forests (RFs) to identify regions-of-interest (ROIs) on ^{18}F-Florbetapir and ^{18}F-FDG PET associated with Montreal Cognitive Assessment (MoCA) score.

Materials and methods: Fifty-seven subjects with significant white matter disease presenting with either transient ischemic attack/lacunar stroke or mild cognitive impairment from early Alzheimer disease, enrolled in a multicenter prospective observational trial, had MoCA and ^{18}F-Florbetapir PET; 55 had ^{18}F-FDG PET. Scans were processed using the MINC toolkit to generate SUV ratios, normalized to cerebellar grey matter (^{18}F-Florbetapir PET) or pons (^{18}F-FDG PET). SUV ratio data and MoCA score were used for supervised training of RFs programmed in MATLAB.

Results: ^{18}F-Florbetapir PETs were randomly divided into 40 training and 17 testing scans; 100 RFs of 1,000 trees, constructed from a random subset of 16 training scans and 20 ROIs, identified ROIs associated with MoCA score: Right posterior cingulate gyrus, Right anterior cingulate gyrus, Left precuneus, Left posterior cingulate gyrus and Right precuneus. Amyloid increased with decreasing MoCA score. ^{18}F-FDG PETs were randomly divided into 40 training and 15 testing scans; 100 RFs of 1,000 trees, each tree constructed from a random subset of 16 training scans and 20 ROIs, identified ROIs associated with MoCA score: Left fusiform gyrus, Left precuneus, Left posterior cingulate gyrus, Right precuneus and Left middle orbitofrontal gyrus. ^{18}F-FDG decreased with decreasing MoCA score.

Conclusions: RFs help pinpoint clinically relevant ROIs associated with MoCA score; amyloid increased and ^{18}F-FDG decreased with decreasing MoCA score, most significantly in the posterior cingulate gyrus.

Keywords: Amyloid, ^{18}F-FDG, PET, random forest, Montreal Cognitive Assessment (MoCA) score

Introduction

Cognitive impairment related to Alzheimer's dementia (AD) is a slowly progressive condition of multi-factorial etiology where the diagnosis is based on clinical evaluation with imaging playing a key supportive role [1-5]. Mild cognitive impairment (MCI) refers to a state where there have been subjective complaints of gradual memory loss for 6 months or more, objective memory loss documented on clinical memory tests and preserved functioning in activities of daily living. It is estimated the prevalence of MCI is 7% in 60-64 year-old subjects rising to 25% in 80-84 year-old subjects. About 10-15% of subjects with MCI progress to dementia annually with more than half progressing to dementia in 5 years [6,7]. Dementia refers to a neurodegenerative condition where loss of cognitive function is sufficient to impair the activities of daily living. The World Health Organization (WHO) estimates 50 million people have dementia worldwide [8]. Typically, screening instruments are used to evaluate subjects with cognitive complaints and guide referral for further investigation. The most common screening instruments are the Mini-Mental State Examination (MMSE) [9] and Montreal Cognitive Assessment (MoCA) [10].

Developed in 2005, the MoCA is a cognitive screening tool that can distinguish patients who are cognitively normal from those with MCI and dementia [10]. It is a one-page 30-point test administered in about 10 minutes, and available at www.mocatest.org. A point is added for subjects with a MoCA score below 30 and 12 or less years of education. In general, MoCA includes more executive functioning tasks than those in the MMSE, making it more sensitive for early cognitive decline. Correlation of MoCA with MMSE is high in cognitively normal and demented subjects, MoCA is often preferred for evaluation of subjects with MCI. Using a cut-off MoCA score of 26 or above as normal, gives sensitivity and specificity for MCI of 90% and 87%, respectively. Also, the specificity of MoCA to exclude subjects with normal cognition is estimated to be over 85% [10]. Recently, it has been suggested that using a score of 26 or above as normal leads to high false positive rates, particularly in older subjects or those with limited education. A meta-analysis by Carson et al., suggested a score of 23 may be preferable to differentiate normal subjects from subjects with MCI [11]. To date, the exact MoCA score to use is a topic of debate.

Although the MoCA cognitive screening tool has gained widespread popularity in clinical practice, there is limited data on anatomical change, amyloid deposition and metabolic function in brain regions associated with MoCA score. Ritter et al. showed a correlation between lower MoCA score and hippocampal atrophy [12]. In this paper, we explore the use of random forests (RFs) with ^{18}F-Florbetapir and ^{18}F-FDG PET to: 1. Suggest regions of the brain predictive of MoCA score and 2. Explore associations of amyloid deposition and glucose uptake in these regions with MoCA score.

Materials and Methods

Fifty-seven subjects with severe white matter hyperintensity volume (WMH), presenting with MCI from early Alzheimer Disease or transient ischemic attack/lacunar stroke, were enrolled in a multicenter prospective observational trial through 9 participating sites as part of the C6 project in the Medical Imaging Network of Canada [13-15]. Of the 57 subjects, 38 were recruited through memory clinics and 19 were recruited through stroke prevention clinics. Inclusion criteria included a MMSE of greater than 20; significant medical or other neurological conditions were cause for exclusion, among other criteria [13,14]. Each subject had a MoCA score, ^{18}F-Florbetapir brain PET and a 3T MRI; 55 also had ^{18}F-FDG brain PET. The MoCA score was considered abnormal if < 25 [16].

Brain PET scans were obtained using scanners at participating sites with consistency of data across sites maintained by adherence to a standard quality assurance program and use of a common imaging protocol, including the main ADNI2 structural protocol [17]. For the ^{18}F-Florbetapir brain PET, the imaging protocol stipulated 370 MBq (10 mCi +/- 10%) ^{18}F-Florbetapir be administered intravenously followed by 20 minutes of dynamic imaging approximately 50 minutes post administration with reconstruction into four 5-minute acquisitions with attenuation and scatter correction. For the ^{18}F-FDG brain PET, 185 MBq (5 mCi +/- 10%) ^{18}F-FDG was to be administered intravenously followed by 30 minutes of dynamic imaging approximately 30 minutes post administration with reconstruction into six 5-minute acquisitions with attenuation and scatter correction. Imaging was transferred to a central site for review. Quantitative data was obtained by processing each brain PET scan with a pipeline programmed

using the MINC toolkit [18] (**Figure 1**). The image acquisitions for each study were averaged, blurred to a common 7-mm full width half maximum (FWHM) to account for differences in camera resolution across sites, and the PET images were registered to the Montreal Neurological Institute template space using the patient MRI as an intermediate step. Masks were used to calculate the SUV ratio (SUVR) for brain regions-of-interest (ROIs), normalized to cerebellar grey matter for the ^{18}F-Florbetapir PET scans and to the pons for the ^{18}F-FDG PET scans. The atlas used for the ROIs included 58 individual brain ROIs, and a composite ROI based on the prefrontal, orbitofrontal, parietal, temporal, anterior cingulate, and posterior cingulate/ precuneus regions (called the Jack mask, which is often affected in AD) [19]. After removing the brainstem and cerebellum from the ROIs due to technical issues, each brain PET scan had 57 associated ROIs also called 57 feature values (56 ROIs and 1 composite ROI).

The SUVR for the ROIs were used for supervised training of two RF scenarios programmed in MATLAB to identify key ROIs on ^{18}F-Florbetapir and ^{18}F-FDG brain PET most associated with MoCA score. In each case, RFs had 1,000 trees, and each tree was created using a subset of 16 cases and 20 features. Specifically, **Scenario 1:** The 57 ^{18}F-Florbetapir brain PET scans were randomly divided into 40 training and 17 testing scans. One hundred RFs (for cross-validation) of 1,000 trees, with each tree constructed using a randomly chosen subset of 16 scans (of the 40 training scans) and 20 features (of the 57 features), were trained according to whether a PET scan was derived from a subject with normal or abnormal MoCA score (< 25 interpreted as abnormal) and the key ROIs used were recorded. **Scenario 2:** The 55 ^{18}F-FDG brain PET scans were randomly divided into 40 training and 15 testing scans, and 100 RFs were trained according to whether a PET scan was derived from a subject with normal or abnormal MoCA score (< 25 interpreted as abnormal) and the key ROIs used were recorded. Two-tailed student's t-tests were computed between SUVRs of the tested groups for the key ROIs. The key ROIs identified by the RFs using the ^{18}F-Florbetapir and ^{18}F-FDG brain PET were then correlated against MoCA score (using a Pearson's correlation coefficient) to explore associations between amyloid deposition and metabolism with cognition. **Figure 2** illustrates how a RF works, while **Figure 3** illustrates how extracted

imaging information using RFs may play a role in knowledge translation to help inform clinical interpretation.

Results

There were 57 subjects (27F, 30M; 57-91 years, mean 76.6 years, standard deviation 8.6 years) with MoCA scores (mean 22.7, standard deviation 4.4) and significant WMH volume (mean 34.7 cm^3 and standard deviation 23.4 cm^3) determined from MRI. Using a MoCA score cut-off of 25 (i.e. score < 25 considered abnormal) for the 57 subjects with a ^{18}F-Florbetapir brain PET, the MoCA score was abnormal in 37 (65%) and normal in 20 (35%) cases; for the 55 subjects with a ^{18}F-FDG brain PET, the MoCA score was abnormal in 35 (64%) and normal in 20 (36%) cases.

Scenario 1: Using a hundred 1,000-tree RFs and all ^{18}F-Florbetapir PETs, the top 5 ROIs at a tree root node (i.e. key ROIs predictive of MoCA score based on amyloid deposition) were the: 1. Right posterior cingulate gyrus, 2. Right anterior cingulate gyrus, 3. Left precuneus, 4. Left posterior cingulate gyrus and 5. Right precuneus, as shown in **Table 1** and **Figure 4**. There was a statistically significant inverse correlation of amyloid deposition with MoCA score in these ROIs, as illustrated in **Figure 5**.

Scenario 2: Using a hundred 1,000-tree RFs and all ^{18}F-FDG PETs, the top 5 ROIs at a tree root node (i.e. key ROIs predictive of MoCA score based on ^{18}F-FDG uptake) were the: 1. Left fusiform gyrus, 2. Left precuneus, 3. Left posterior cingulate gyrus, 4. Right precuneus and 5. Left middle orbitofrontal gyrus, as shown in **Table 2** and **Figure 6**. There was a trend towards a direct correlation of ^{18}F-FDG uptake with MoCA score, most notably in the left posterior cingulate gyrus, as illustrated in **Figure 7**.

Discussion

The clinical syndrome associated with AD, a frequent pathology in autopsies of subjects with cognitive impairment, is thought to be related to the progressive accumulation of amyloid plaques and tau tangles often co-morbid with additional proteinopathies and vasculopathies [5]. This results in

dysfunction of neural networks with gradual cognitive decline, evidenced by episodic memory loss, language, visuo-spatial and executive difficulties [20-22].

Although the diagnosis of cognitive impairment and dementia has long been made clinically, recently there has been a push for greater emphasis to be placed on the presence of imaging and/or cerebral spinal fluid (CSF) abnormalities. To wit, in 2016, Jack et al. proposed the "A/T/N" system in subjects with suspected dementia in an effort to improve clinical consistence in diagnosis., "A" is for amyloid positivity (on amyloid PET or CSF $A\beta_{42}$), "T" for tau positivity (on tau PET or CSF phospho tau) and "N" for neurodegeneration or neuronal injury (on ^{18}F-FDG PET, MRI or CSF total tau) [23]. Further, in 2018, the National Institute on Aging and Alzheimer's Association (NIA-AAA) research framework suggested Alzheimer's Dementia (AD) be defined by biomarkers such as Aβ deposition, pathologic tau and neurodegeneration, irrespective of clinical manifestations [24].

In addition, there has been a recent proliferation in the use of machine learning (ML) algorithms to identify features on anatomic and molecular imaging that discriminate cognitive status and suggest outcome. For example, brain MRI features such as cortical thickness, among others, have been used to classify cognitively normal subjects from those with MCI and/or dementia [25,26]. Blazhenets et al. identified a cerebral metabolic pattern on ^{18}F-FDG PET associated with conversion from MCI to AD [27]. While, a host of ML algorithms have been assayed, one that has shown promise, particularly with small datasets, is the RF. In a systematic review, Sarica et al., suggested RFs could distinguish AD from healthy controls with accuracy ~90% and could distinguish MCI from healthy controls with accuracy ~ 80% [28].

An RF is a supervised ML algorithm that uses a collection of decision trees, to sort data. For example, a feature value for a PET scan such as the SUVR for a specific brain ROI is used by a tree in the forest and a decision is made to branch left or right, based on a trained condition chosen to separate the data into two classes with greatest classification accuracy. To train a RF, a subset of cases from the complete dataset and a subset of features from the complete set of features is randomly chosen. A tree in the RF is then built using this random subset of cases and features for training. This is repeated for all the

trees in the RF. Each new case in the testing dataset is then evaluated by all the trees in the RF with the final decision being the classification that is most common after inspection of all of the trees. Two of the advantages of RFs are that: 1. they are tolerant to overfitting and 2. can pinpoint key imaging features for further evaluation. Or, in other words, features appearing most commonly at a root node of a tree, that are key for a classification outcome.

Our group recently used a RF, to help classify ^{18}F-Florbetapir brain PET as positive or negative for amyloid deposition [29]. In this paper, we use RFs not to classify scans as positive or negative for disease but rather to identify brain ROIs on ^{18}F-Florbetapir and ^{18}F-FDG brain PET associated with MoCA score. For the purposes of our analysis we chose a cut-off score < 25 as abnormal. Recognizing the ongoing debate regarding the choice of MoCA score used to classify a subject as cognitively normal versus cognitively impaired/ abnormal, we based our choice on the recommended cut-off for a Canadian sample (since all of the subjects included in this study were Canadian) [16]. On ^{18}F-Florbetapir brain PET, the top 5 brain ROIs associated with MoCA score were the: right and left precuneus, right and left posterior cingulate gyrus, right anterior cingulate gyrus, (**Table 1**) with a statistically significant inverse correlation between the SUVR in these ROIs and MoCA score (**Figure 5**). Specifically, we found increased amyloid deposition in these ROIs correlated with decreased cognition on MoCA. This is consistent with results suggested by the literature [30,31]. For ^{18}F-FDG brain PET, the top 5 brain ROIs associated with MoCA score were the: left and right precuneus, left posterior cingulate gyrus, left fusiform gyrus and left middle orbitofrontal gyrus (**Table 2**) with a trend towards a direct correlation between the SUVR in these ROIs and MoCA score (**Figure 7**). Notably, decreased ^{18}F-FDG uptake in the left posterior cingulate gyrus correlated with decreased MoCA score, an AD signature area for PET hypometabolism [30].

In 2010, Jack et al. published their hypothetical model of dynamic biomarkers of the Alzheimer's pathological cascade in which amyloid accumulates and then metabolism declines as cognitive function decreases [32]. ^{18}F-Florbetapir brain PET is thought to be both sensitive and specific for distinguishing none to sparse from moderate to frequent amyloid plaque (87% and 95% respectively) [33]. Today, scans

are clinically read as positive or negative for amyloid deposition and there is a debate if information regarding regional amyloid deposition should be reported. Quantitation may emphasize either an overall amyloid burden and/or the regional nature of accumulation over time. Also, while amyloid plaque may be seen in cognitively normal subjects [34], interestingly, amyloid deposition may predate clinically apparent cognitive decline by several years. It is possible that, at least early on, evaluation of amyloid deposition in specific ROIs rather than overall amyloid burden may more closely parallel cognitive change, although further data is needed to confirm this.

^{18}F-FDG brain PET is thought to be both sensitive (93%) and specific (93%) for differentiating normal controls from subjects with AD [35]. Classically, a regional interpretation of imaging is used and the posterior cingulate gyrus, precuneus, temporoparietal and frontal regions are typically affected first, with preservation of the primary visual cortex, sensorimotor cortex and basal ganglia [27,36]. This was corroborated by our findings. While reduced neocortical glucose metabolism may be detected prior to clinical symptoms, similar to amyloid deposition, abnormalities in ^{18}F-FDG uptake are thought to be more closely correlated in time [37].

Conclusions

In a population consisting primarily of subjects with MCI/ mild AD and significant WMH volume, this investigation suggests RFs may pinpoint clinically relevant brain ROIs, such as the posterior cingulate gyrus, that correlate with abnormal MoCA score. Increasing amyloid accumulation and decreasing metabolism was seen in these ROIs as cognitive impairment became more pronounced.

References

[1] McKhann GM, Knopman DS, Chertkow H, et al. The diagnosis of dementia due to Alzehimer's disease: recommendations from the National Institute on Aging – Alzheimer's Association workgroups on diagnostic guidelines for Alzheimer's disease. *Alzheimers Dement*. 2011;7:263-269.

[2] Albert MS, Dekosky ST, Dickson D, et al. The diagnosis of mild cognitive impairment due to Alzheimer's disease: recommendations from the National Institute on Aging – Alzheimer's Association workgroups on diagnostic guidelines for Alzheimer's disease. *Alzheimers Dement*. 2011;7:270-279.

[3] Sperling RA, Aisen P, Beckett L, et al. Toward defining the preclinical stages of Alzheimer's disease: recommendations from the National Institute on Aging – Alzheimer's Association workgroups on diagnostic guidelines for Alzheimer's disease. *Alzheimers Dement*. 2011;7:280-292.

[4] Gauthier S, Patterson C, Chertkow H, et al. 4th Canadian Consensus Conference on the Diagnosis and Treatment of Dementia. *Can J Neurol Sci*. 2012;39(Suppl 5):S1-S8.

[5] Kapasi A, DeCarli C and Schneider JA. Impact of multiple pathologies on the threshold for clinically overt dementia. *Acta Neuropathol*. 2017;134(2):171-186.

[6] Gauthier S, Reisberg B, Zaudig M, et al. Mild cognitive impairment. *Lancet* 2006; 367:1262–1270

[7] Petersen RC, Lopez O, Armstrong MJ, et al. Practice guideline update summary: Mild cognitive impairment. *Neurology.* 2018; 90:1-10

[8] Dementia. World Health Organization website. http://www.who.int/mediacentre/factsheets/fs362/en/. Updated May 14, 2019. Accessed July 9, 2019.

[9] Folstein MF, Folstein SE, McHugh PR. «Mini-mental state». A practical method for grading the cognitive state of patients for the clinician. J Psychiatr Res. 1975;12(3):189-198.

[10] Nasreddine Z, Phillips N, Bedirian V, et al. The Montreal Cognitive Assessment, MoCA: A Brief Screening Tool for Mild Cognitive Impairment. *J Am Geriatr Soc.* 2005;53:695-699.

[11] Carson N, Leach L, Murphy KJ. A re-examination of Montreal Cognitive Assessment (MoCA) cutoff scores. *Int J Geriatr Psychiatry.* 2018;33:379-388.

[12] Ritter A, Hawley N, Banks S, et al. Cognitive Assessment Memory Scores and Hippocampal Volume in a Neurodegenerative Disease Sample. *J Alzheimers Dis.* 2017;58:695-699.

[13] MITNEC Theme C: Imaging Trials in Neurology. MITNEC website. http://www.mitnec.org/index.php?option=com_content&view=category&layout=blog&id=49&Itemid=116. Accessed July 9, 2019.

[14] Amyloid and Glucose PET Imaging in Alzheimer and Vascular Cognitive Impairment Patients With Significant White Matter Disease (MITNEC C6): NCT02330510. https://www.clinicaltrials.gov/ct2/show/NCT02330510?term=NCT02330510&rank=1. Updated November 27, 2017. Accessed July 8, 2019.

[15] Fazekas F, Chawluk JB, Alavi A, et al. MR signal abnormalities at 1.5T in Alzheimer's dementia and normal aging. *AJR Am J Roentgenol*. 1987;149(2):351-356.

[16] Smith EE, O'Donnell M, Dagenais G, et al. Early cerebral small vessel disease and brain volume, cognition, and gait. Ann Neurol. 2015;77(2):251-261

[17] Petersen R, Weiner M. ADNI 2 Procedures Manual. http://adni.loni.usc.edu/wp-content/uploads/2008/07/adni2-procedures-manual.pdf. Accessed July 9, 2019.

[18] MINC Toolkit. McConnell Brain Imaging Centre. http://www.bic.mni.mcgill.ca/ServicesSoftware/MINC. Updated August 13, 2014. Accessed July 9, 2019.

[19] Jack CR Jr., Lowe VJ, Senjem ML, et al. ^{11}C PiB and structural MRI provide complementary information in imaging of Alzheimer's disease and amnestic mild cognitive impairment. *Brain*. 2008;131:665-680.

[20] Shinohara M, Fujioka S, Murray M, et al. Regional distribution of synaptic markers and APP correlate with distinct clinicopathological features in sporadic and familial Alzheimer's disease. *Brain*. 2014;137:1533-1549.

[21] Crews L, Masliah E. Molecular mechanisms of neurodegeneration in Alzheimer's disease. *Hum Mol Genet*. 2010;19(R1):R12-R20.

[22] Braak H and Braak E. Neuropathological stageing of Alzheimer-related changes. *Acta Neuropathol*. 1991;82:239-259.

[23] Jack CR, Jr., Bennett DA, Blennow K, et al. A/T/N/: An unbiased descriptive classification scheme for Alzheimer disease biomarkers. *Neurology*. 2016;87(5):539-547.

[24] Jack CR, Jr., Bennett DA, Blennow K, et al. NIA-AA Research Framework: Towards a Biological Definition of Alzheimer's Disease. *Alzheimers Dement*. 2018;14(4):535-562.

[25] de Vos F, Schouten TM, Hafkemeijer A, et al. Combining multiple anatomical MRI measures. improves Alzheimer's disease classification. *Hum Brain Mapp*. 2016;37:1920-1929.

[26] Dimitriadis SI, Liparas D, Tsolaki MN, Alzheimer's Disease Neuroimaging Initiative. Random forest feature selection, fusion and ensemble strategy: combining multiple morphological MRI measures to discriminate among health elderly, MCI, cMCI and Alzheimer's disease patients: from the Alzheimer's disease neuroimaging initiative (ADNI) database. *J Neurosci Methods*. 2018;302:14-23.

[27] Blazhenets G, Yilong M, Sorensen A, et al. Principal component analysis of brain metabolism predicts development of alzheimer dementia. *J Nucl Med*. 2019;60:837-843.

[28] Sarica A, Cerasa A, Quattrone A. Random Forest Algorithm for the Classification of Neuroimaging Data in Alzheimer's Disease: A Systematic Review. *Front Aging Neurosci*. 2017;9:329.

[29] Zukotynski K, Gaudet V, Kuo P, et al. The use of random forests to classify amyloid brain PET. *Clin Nucl Med*. 2019;44(10):784-788.

[30] Palmqvist S, Scholl M, Strandberg O, et al. Earliest accumulation of beta-amyloid occurs within the default-mode network and concurrently affects brain connectivity. *Nat Commun*. 2017;8(1):1214.

[31] Buckner RL, Snyder AZ, Shannon BJ, et al. Molecular, structural, and functional characterization of Alzheimer's disease: Evidence for a relationship between default activity, amyloid, and memory. *J Neurosci*. 2005;25(34):7709-7717.

[32] Jack CR Jr. Knopman DS, Jagust WJ, et al. Hypothetical model of dynamic biomarkers of the Alzheimer's pathological cascade. *Lancet Neurol.* 2010;9:119-128

[33] Clark CM, Pontecorvo MJ, Beach TG, et al. Cerebral PET with florbetapir compared with neuropathology at autopsy for detection of neuritic amyloid-beta plaques: a prospective cohort study. *Lancet Neurol*. 2012;11:669-678.

[34] Aizenstein HJ, Nebes RD, Saxton JA, et al. Frequent amyloid deposition without significant cognitive impairment among the elderly. *Arch Neurol*. 2008;65:1509-1517.

[35] Herholz K, Salmon E, Perani D, et al. Discrimination between Alzheimer dementia and controls by automated analysis of multicenter FDG PET. *Neuroimage*. 2002;17:302-316.

[36] Mattis PJ, Niethammer M, Sako W, et al. Distinct brain networks underlie cognitive dysfunction in Parkinson and Alzheimer diseases. *Neurology*. 2016;87:1925-1933.

[37] Chatelat G, Desgranges B, de ISV, et al. Mild cognitive impairment : can FDG-PET predict who is to rapidly convert to Alzheimer's disease? *Neurology*. 2003;60:1374-1377.

Figure 1: Image-processing pipeline using the MINC toolkit: Negative ^{18}F-FDG PET with associated MRI is shown in (A-E) and positive ^{18}F-FDG PET with associated MRI is shown in (F-J). (A,F) Averaged and blurred PET image. (B,G) Patient MRI. (C,H) Patient PET registered to template space, showing SUVR on a colour scale with blue indicating lower SUVR and red indicating higher SUVR. (D,I) MRI template. (E,J) Example ROI mask superimposed on PET image.

Figure 2: Simplified illustration of a RF being used to help identify brain ROIs on ^{18}F-Florbetapir associated with MoCA score. (A) 10 training cases, each with 6 features and 2 output classes. (B) RF with 3 trees, each trained using a randomly selected subset of 4 cases and 3 features; root nodes are the right posterior cingulate gyrus, left precuneus, and left posterior cingulate gyrus.

Figure 3: Illustration of a machine learning algorithm being used to help clinical interpretation.

Figure 4: ^{18}F-Florbetapir PET regions-of-interest most commonly associated with abnormal MoCA score.

Figure 5: Activity (SUVR) in regions-of-interest on ^{18}F-Florbetapir PET, plotted versus MoCA score. (A) Left posterior cingulate gyrus. (B) Right posterior cingulate gyrus. (C) Left anterior cingulate gyrus. (D) Right anterior cingulate gyrus. (E) Left precuneus. (F) Right precuneus.

Figure 6: ^{18}F-FDG PET regions-of-interest most commonly associated with abnormal MoCA score.

Figure 7: Activity (SUVR) in regions-of-interest on ^{18}F-FDG PET, plotted versus MoCA score. (A) Left fusiform gyrus. (B) Right fusiform gyrus. (C) Left precuneus. (D) Right precuneus. (E) Left posterior cingulate gyrus. (F) Right posterior cingulate gyrus.

Figure 1

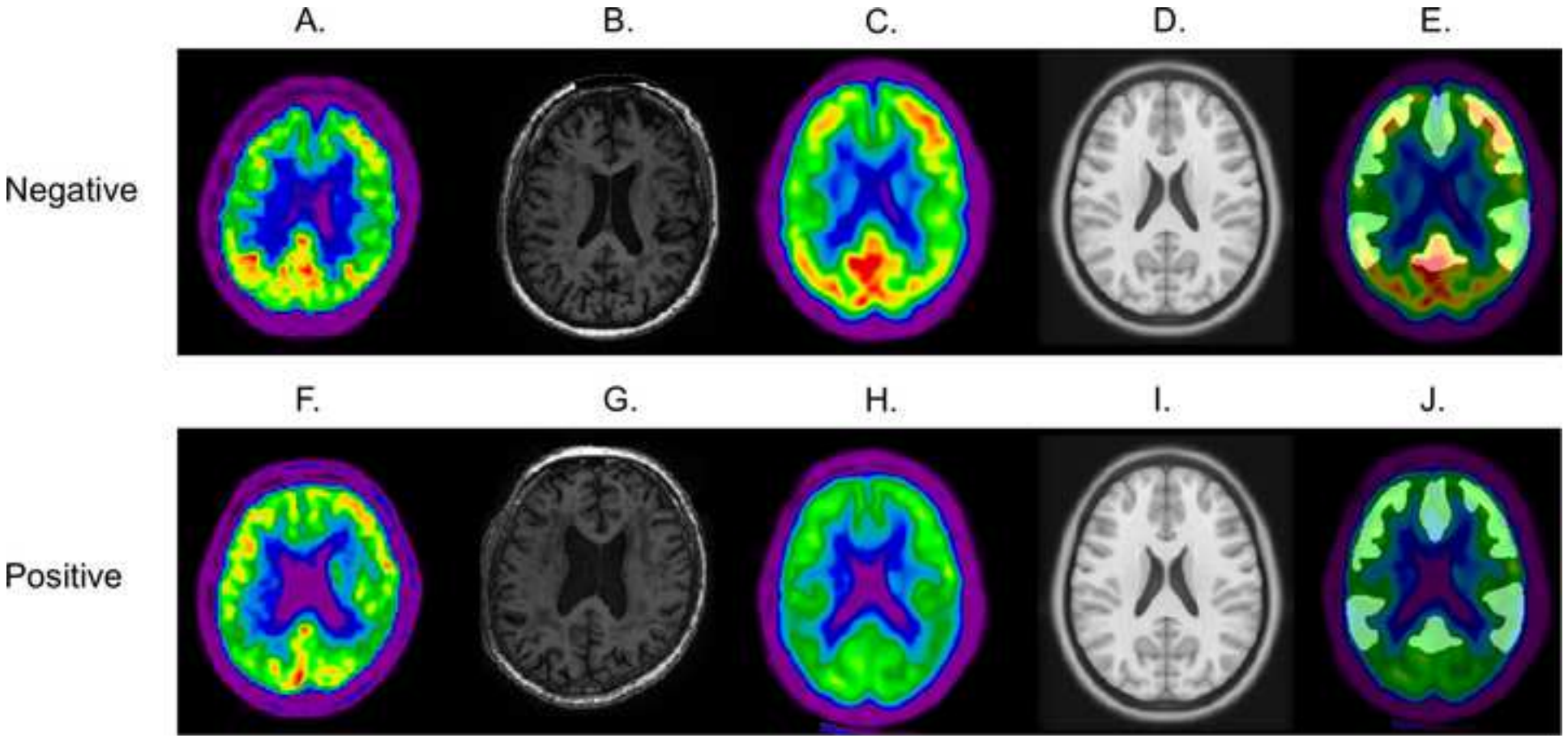

Figure 2

A.

	L post cing	R post cing	L prec	R prec	L ant cing	R ant cing	MoCA POS or NEG
1	1.08	1.10	1.15	1.11	0.91	0.99	POS
2	1.56	1.75	1.63	1.61	1.37	1.40	POS
3	1.55	1.51	1.43	1.38	1.23	1.26	POS
4	1.95	1.84	1.70	1.87	1.10	1.26	POS
5	2.10	2.09	1.73	1.60	1.68	1.71	POS
6	1.43	1.35	1.42	1.27	1.20	1.17	NEG
7	1.12	1.21	0.98	0.94	1.12	1.27	NEG
8	1.74	1.70	1.36	1.36	1.59	1.33	NEG
9	1.29	1.25	1.31	1.24	1.39	1.32	NEG
10	0.88	0.92	0.89	0.90	0.83	0.87	NEG

B.

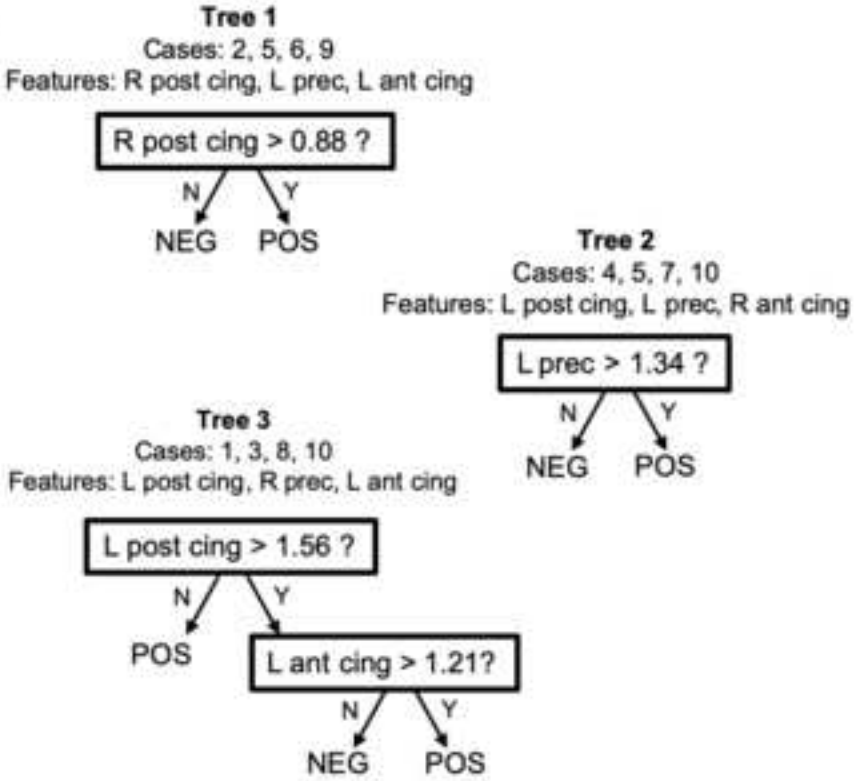

Figure 3

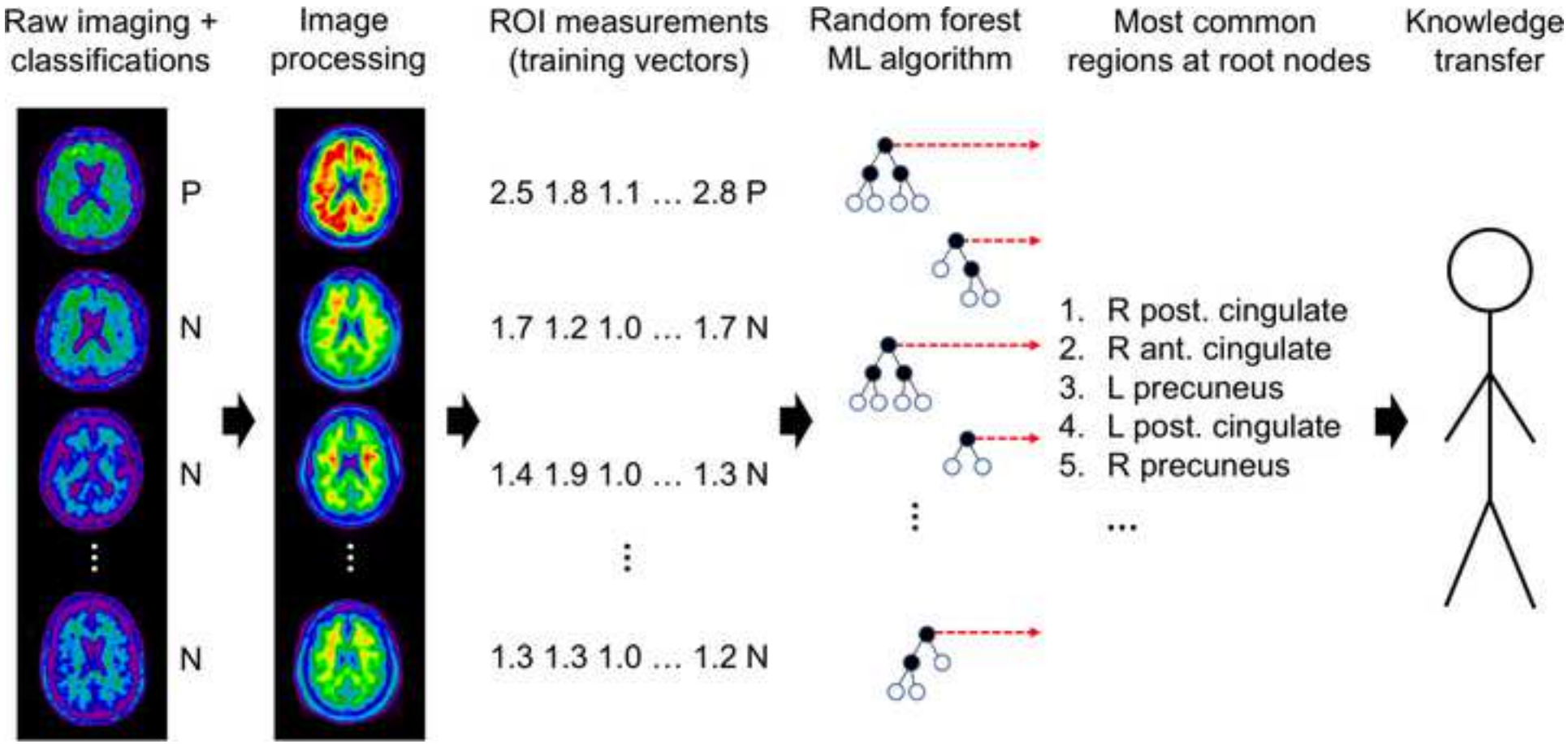

Figure 4

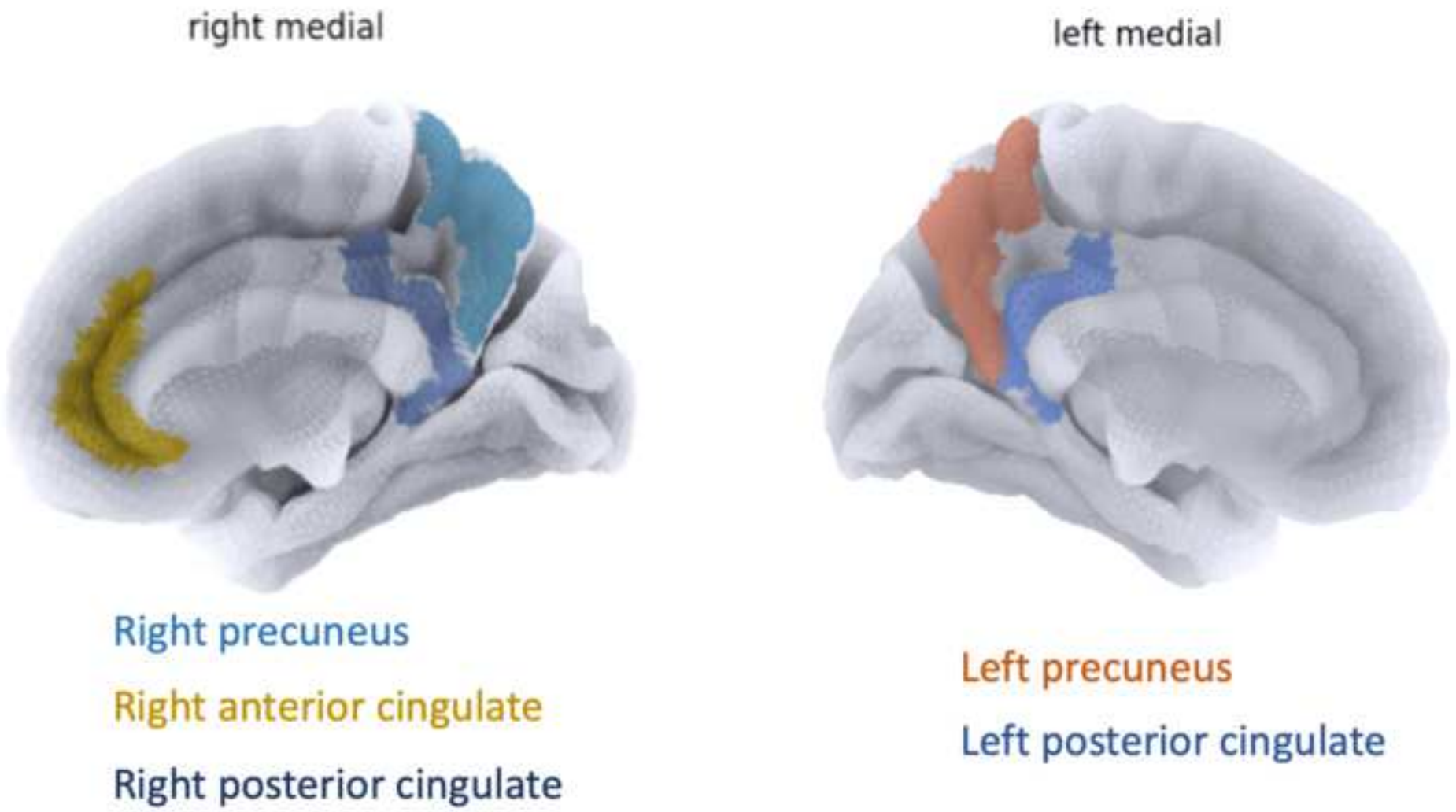

Figure 5

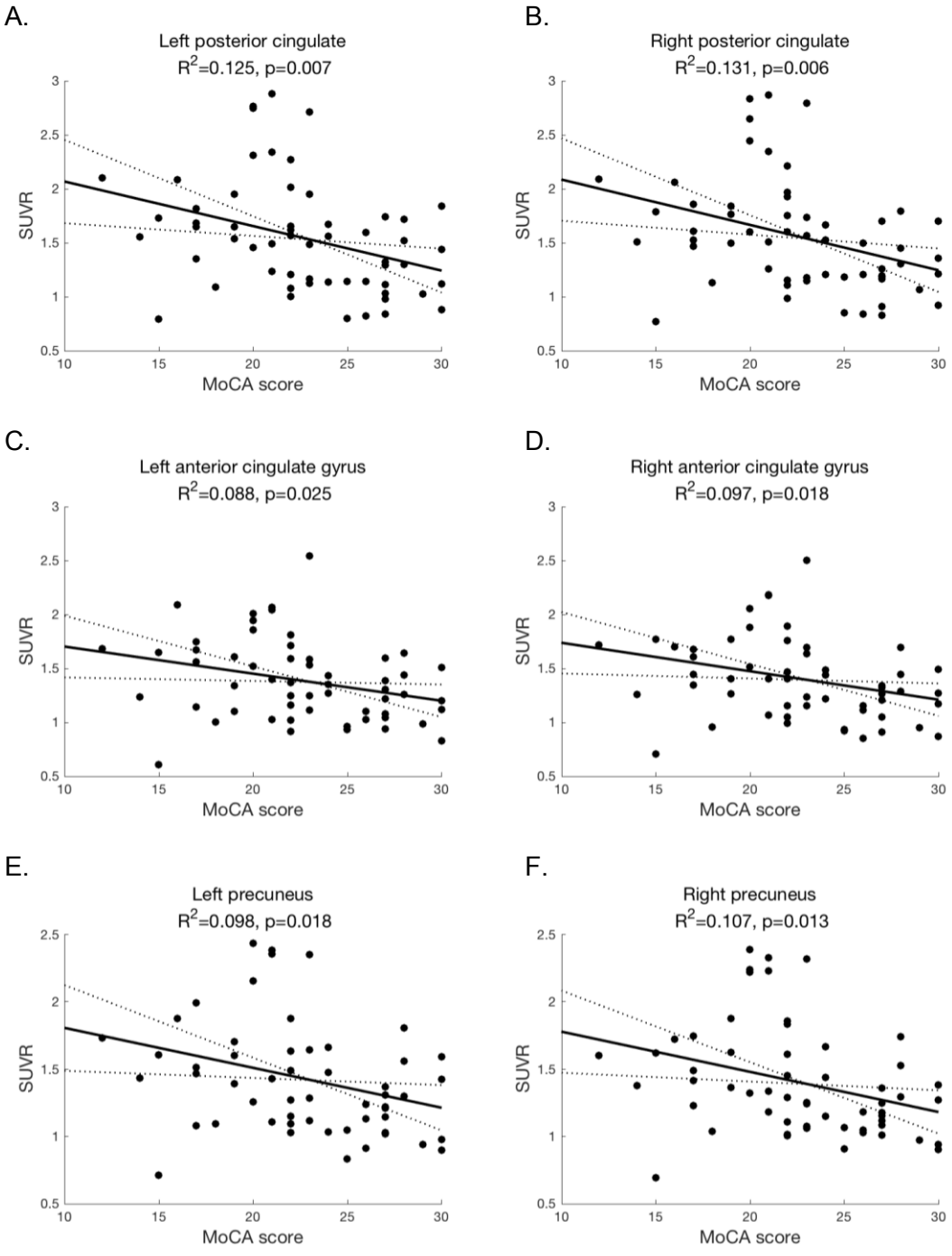
A.
Left posterior cingulate
R^2=0.125, p=0.007
B.
Right posterior cingulate
R^2=0.131, p=0.006
C.
Left anterior cingulate gyrus
R^2=0.088, p=0.025
D.
Right anterior cingulate gyrus
R^2=0.097, p=0.018
E.
Left precuneus
R^2=0.098, p=0.018
F.
Right precuneus
R^2=0.107, p=0.013
SUVR
MoCA score

Figure 6

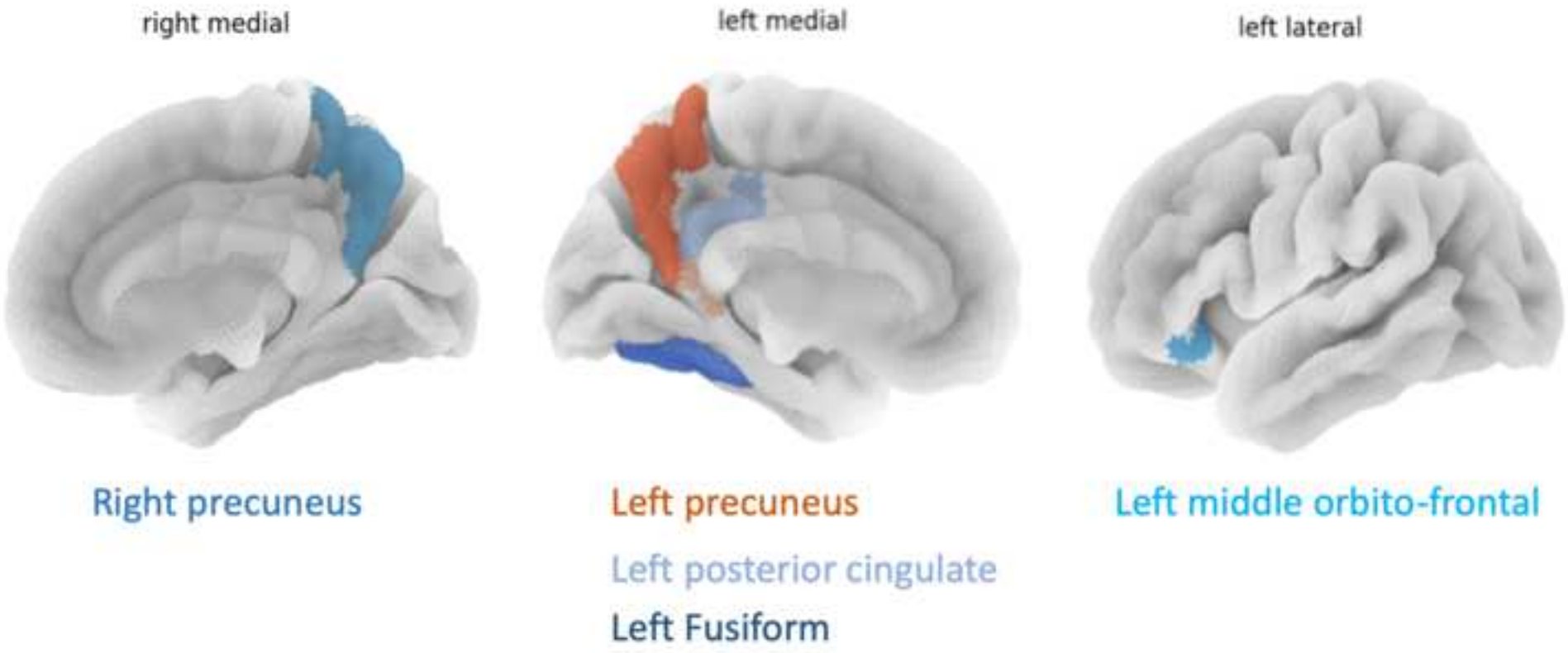

Figure 7

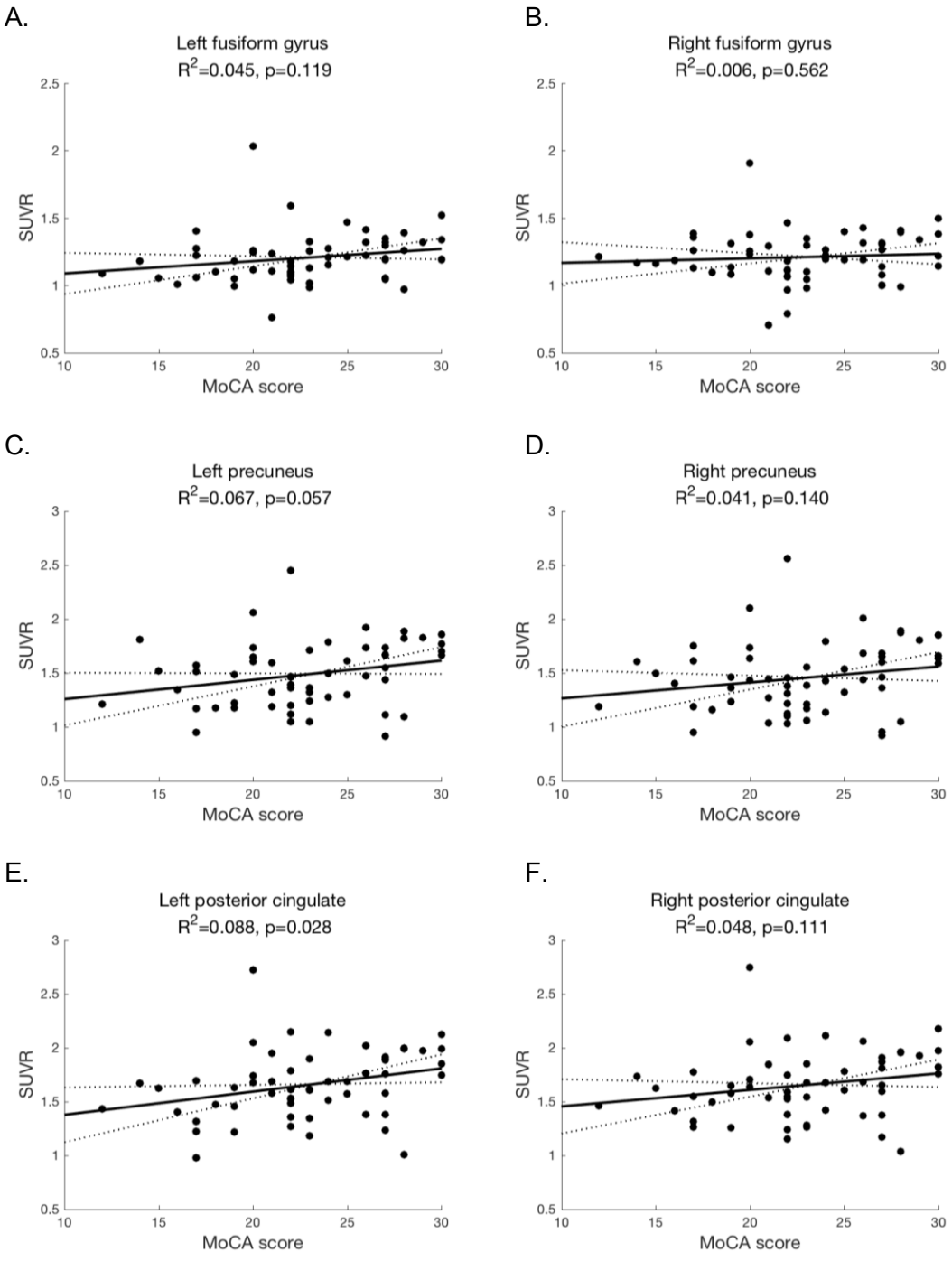
A.
Left fusiform gyrus
R^2=0.045, p=0.119
B.
Right fusiform gyrus
R^2=0.006, p=0.562
C.
Left precuneus
R^2=0.067, p=0.057
D.
Right precuneus
R^2=0.041, p=0.140
E.
Left posterior cingulate
R^2=0.088, p=0.028
F.
Right posterior cingulate
R^2=0.048, p=0.111
SUVR
MoCA score

Table 1

Table 1: Features commonly found at the root node in 100 RFs each with 1,000 trees trained to sort ^{18}F-Florbetapir PET into one of two categories: MoCA score <25 or ≥25, using 16 randomly selected scans and 20 randomly selected features (SUVR in brain ROIs) per tree. Average SUVRs and 2-tailed Student's t test p-value using common variance assumption are given. Bold text indicated higher values.

Region	**Number of instances at a root node**	**Average SUVR MoCA score ≥25**	**Average SUVR MoCA score <25**	**p-value**
Right posterior cingulate	6945	1.23	**1.73**	$3x10^{-4}$
Right anterior cingulate gyrus	5643	1.18	**1.52**	$6x10^{-4}$
Left precuneus	5377	1.19	**1.55**	$2x10^{-3}$
Left posterior cingulate	5353	1.23	**1.71**	$5x10^{-4}$
Right precuneus	4356	1.17	**1.52**	$1x10^{-3}$

Table 2

Table 2: Features commonly found at the root node in 100 RFs each with 1,000 trees trained to sort ^{18}F-FDG PET into one of two categories: MoCA score <25 or ≥25, using 16 randomly selected scans and 20 randomly selected features (SUVR in brain ROIs) per tree. Average SUVRs and 2-tailed Student's t test p-value using common variance assumption are given. Bold text indicated higher values.

Region	**Number of instances at a root node**	**Average SUVR MoCA score ≥ 25**	**Average SUVR MoCA score < 25**	**p-value**
Left fusiform gyrus	5724	**1.26**	1.17	0.08
Left precuneus	5018	**1.59**	1.43	0.06
Left posterior cingulate	4558	**1.74**	1.60	0.14
Right precuneus	3675	**1.55**	1.40	0.10
Left middle orbitofrontal gyrus	3441	**1.31**	1.24	0.38